Impact of Accurate Motion-Corrected Statistical Reconstruction on Dynamic PET Kinetic Parameter Estimation

A. Rahmim, K. Dinelle, S. C. Lidstone, S. Blinder, J. C. Cheng, G. Topping, H. Vajihollahi, D. F. Wong, V. Sossi

***Abstract*— With continuing improvements in spatial resolution of PET scanners, small subject movements become a significant source of resolution degradation. This work assesses the impact of an accurate motion correction (MC) method, modeling the 'motion-induced' interaction of lines-of-response (LORs) inside and outside the field-of-view, on the task of kinetic parametric estimation in high resolution dynamic PET. Following extensive prior phantom and simulation validations, we performed external tracking of motion using the Polaris camera on ten Parkinson's decease (PD) subjects scanned on the high resolution research tomograph (HRRT). The resulting time-activity curves (TACs) generated from dynamic frames were compared in terms of (i) increased binding potential (BP) values as well as (ii) reduced χ^2 variations in the TAC fitting task, due to hypothesized increased effective-resolution and accuracy achieved via accurate MC. The Wilcoxon non-parametric matched-pair signed-rank test was applied to the BP as well as χ^2 values before and after MC, and demonstrated significant changes for the overall striatal region as well as a number of individual striatal regions-of-interest (ROIs). For the BP values, the increases were shown to be more significant for the subset of subjects (6 out of 10) which exhibited maximum displacements larger than the resolution (2.5mm) of the HRRT. Additionally, the method was demonstrated as a possible approach to standard clinical imaging with no, or minimal, head restraint.**

I. Introduction

With continuing improvements in spatial resolution of PET scanners, small subject movements during PET imaging become a significant source of resolution degradation. In the context of brain imaging, a number of head restraint methods have been used, such as thermoplastic masks or velcro straps, which lower the amount of motion but are not able to eliminate it [16] (methods that are too restrictive will be less acceptable to volunteers, and also potentially introduce further movement to relieve discomfort). Even with head restraints, typical translations in the range of 5-20 mm and rotations of 1-4° are observed, depending on the type of mask and the duration of scan (e.g. see [6], [12], [17]). Consequently, several methods for motion tracking and correction have been proposed over the years (for an elaborate review, see [27]). Below, we briefly outline some of these methods in order to motivate our choice of motion correction scheme.

A. Rahmim and D. F. Wong are with the Division of Nuclear Medicine, Department of Radiology, Johns Hopkins University, Baltimore MD 21205 (e-mail arahmim1@jhmi.edu, pvcorrection@yahoo.com, dfwong@jhmi.edu).

K. Dinelle, J. C. Cheng, G. Topping and V. Sossi are with the Department of Physics and Astronomy, University of British Columbia, Vancouver BC V6T 1Z1 (e-mail kdinelle@phas.ubc.ca, jcheng@phas.ubc.ca, vesna@phas.ubc.ca).

S. C. Lidstone and S. Blinder are with Pacific Parkinson's Research Centre, Vancouver BC V6T 1Z1 (e-mail lidstone@interchange.ubc.ca, blinder@phas.ubc.ca).

H. Vajihollahi is with the Department of Mechanical Engineering, McMaster University, Hamilton ON L8S 4L8 (e-mail vajihollahi@hotmail.com).

A. Motion Correction Strategies

An ongoing trend consists of using external tracking of motion; this is because motion correction (MC) strategies that rely exclusively on the emission data may be inadequate for robust routine usage, since (i) they depend on the quality of the scan data including noise characteristics and (ii) they assume the activity distribution does not significantly change within the frames into which the data are divided *a priori*. Improved success is achieved with methods that rely on motion information provided by an external motion-tracking device (e.g. the Polaris system [6], which was also used in this work as elaborated in Sec. II). In dynamic PET imaging, these have been shown to result in improved parametric PET images [35], as well as improved statistical performance, particularly reduction in parameter test-retest variability [4].

Reconstruction approaches, in the context of rigid motion (e.g. brain PET), that make use of tracked motion information have been reviewed in [27], and include the method of multiple acquisition frames (MAFs) [7], [17], use of de-convolution post-processing [20] and modeling of entire motion in the system matrix of the EM algorithm [9], [25]. A novel and potentially more accurate approach to MC has been to correct individual lines-of-response (LORs) for motion (i.e. event-driven MC) [12], [21]: this is easily applicable to scanners with list-mode acquisition capabilities. However, as elaborated in [24], [26], this approach does not address the following two issues:

(**Issue-1**) An event that is normally in the field-of-view (FoV) can fall outside the FoV because of motion, thus not being detected.

(**Issue-2**) An event that is normally not in the FoV, may fall within the FoV because of motion (and is conventionally discarded).

These two effects can occur in the axial direction, and also for scanners with gaps between detector heads. As such, in the first case, following MC, the subset of events that were lost due to motion are conventionally not accounted for in the system matrix, while in the second case, following MC,

1-4244-0923-3/07/$25.00 ©2007 IEEE.

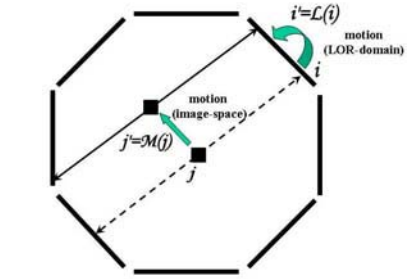

(a)

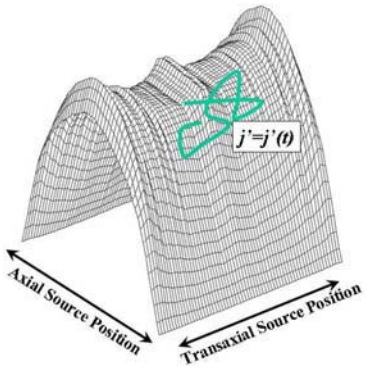

(b)

Fig. 1. (a) Definition of the image-space motion operator $\mathcal{M}()$; (b) The overall sensitivity factor $\overline{s}_j$ for a voxel j can be calculated in the *image-space* by weighted evaluation of the conventional sensitivity term along the trajectory j' of the voxel.

a number of events are aligned outside the FoV (and are most often discarded). Neglecting *issue-1* can produce image artifacts [3], [22]–[24] while discarding events in *issue-2* can result in a decrease in the signal-to-noise ratio (SNR).

Qi and Huesman [22] proposed a list-mode reconstruction approach that addressed these issues via modeling of motion into the system matrix of the EM algorithm. Within the contexts of both histogram-mode and list-mode algorithms, Rahmim *et al.* [24] proposed a framework for feasible motion-incorporated reconstruction of large volumes of high-resolution PET data, which also resolved the issues outlined above. In contrast, the methods proposed in [23] and [3] addressed *issue-1* only, involved pre-correction of sinogram bins for the effect of motion with potential noise amplification issues [3], and were more computationally intense (entirely based in the projection-space), as discussed in [27].

The approach in [24] was later extended [26] to accurately incorporate scatter and random correction terms in the presence of motion. This method will be used for all motion-corrected reconstructions done within this paper, and its performance evaluated in terms of kinetic parameter estimation. To summarize, the algorithm starts by dividing a given scan (of duration T) into Q motion-related time intervals (t=1...Q) each with a duration ΔT_t within which motion is limited below a small, negligible threshold. Then, we define an operator $\mathcal{M}_t()$ which models the movement of any voxel j to the new position j' at time t (Fig. 1a). Defining N_i and A_i as the normalization and attenuation factors along an LOR i, with g_{ij} denoting the geometric probability of detection between a voxel j and LOR i, we have demonstrated mathematically [24] that (i) *if* the data are pre-corrected for attenuation, and (ii) *all* detected events are taken into consideration (i.e. *issue-2* is not neglected), the overall sensitivity correction term is given by:

$$\overline{s}_j = \sum_{t=1}^{Q} s_{j'} \frac{\Delta T_t}{T} \quad \text{with} \quad j' = \mathcal{M}_t(j) \tag{1}$$

Here s_j is the standard sensitivity term ($s_j = \sum_{i=1}^{I} g_{ij} N_i$), which can be calculated by image-space averaging of the sensitivity term, as depicted in Fig. 1b. The overall statistical EM algorithm incorporating MC is then given by [26]:

$$f_j^{m+1} = \frac{f_j^m}{T\overline{s}_j} \sum_{i=1}^{I} g_{ij} \frac{n_i/A_i}{\sum_{b=1}^{J} g_{ib} f_b^m + \frac{\widetilde{R}_i}{A_i} + \frac{\widetilde{S}_i}{A_i}} \tag{2}$$

wherein f_j^m denotes the activity (i.e. emission *rate*) in voxel j (j=1...J) estimated at the m^{th} iteration, n_i refers to the number of events *binned* (i.e. following MC) along LOR i (i=1...I), and $\widetilde{S}_i$ and $\widetilde{R}_i$ are given [26] by the estimated rates of normalized scatter and random events if the object did not move during the study. $\widetilde{S}_i$ is shown to be well approximated by the standard Watson single scatter simulation (SSS) method performed on MC sinograms, while $\widetilde{R}_i$ is estimated by normalizing the standard estimated detected randoms R_i^{det}:

$$\widetilde{R}_i \equiv \begin{cases} \frac{R_i^{det}}{N_i} & \text{LOR } i \text{ in FoV (i.e. can be detected)} \\ extrapolate\left\{\frac{R_i^{det}}{N_i}\right\} & \text{otherwise} \end{cases} \tag{3}$$

which for LORs outside the FoV (e.g. axially, or along gaps) is obtained by extrapolating to nearby LORs.

Similarly, the list-mode image reconstruction [18], [19] counter-part, as investigated in this work, is given by:

$$f_j^{m+1} = \frac{f_j^m}{T\overline{s}_j} \sum_{k=1}^{K} g_{ij} \frac{1/A_i}{\sum_{b=1}^{J} g_{ib} f_b^m + \frac{\widetilde{R}_i}{A_i} + \frac{\widetilde{S}_i}{A_i}} \tag{4}$$

wherein summation is performed over all list-mode events k=1...K.

B. Phantom and simulation studies

In [24], the accuracy of our list-mode MC framework (Eq. 4) was extensively analyzed and validated. This was achieved via: (1) phantom studies as well as (2) realistic simulations of the high resolution research tomograph (HRRT) using a combined SimSET/GATE simulation method and a new mathematical brain phantom. Quantitatively, it was observed that the proposed method resulted in improved contrast vs. noise as well as bias vs. noise curves as compared with no motion correction or the purely event-driven method. In addition, it was able to eliminate artifacts observed when using the latter approach, as it takes into account presence of detector gaps in the HRRT. In the present work, we investigate effects of this MC framework on human brain PET studies.

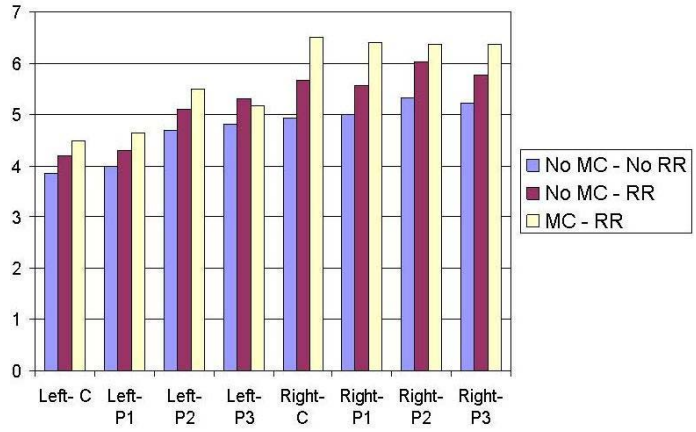

Fig. 2. Comparison of BP values (as described in Sec. II-D.2) obtained via different reconstruction methods for a particular PD subject studied in this work: values are shown for various striatal ROIs, namely the right and left caudate (C), anterior putamen (P1), intermediate putamen (P2), and posterior putamen (P3), as elaborated in Sec. II-D.1.

C. Parallels with Incorporation of Resolution-Recovery

An important motivation for this study has been to perform a thorough, quantitative inspection of differences encountered without and with MC in kinetic parameter estimation. In [30], Sureau *et al.* have performed such a quantitative comparison for reconstructions without and with resolution recovery (RR), incidentally performed on the HRRT scanner also used in this work. For both MC and RR, it is intuitive to hypothesize (see Sec. II-D.2) an increased effective resolution for the scanner, predicting increased binding potential (BP) values, as confirmed in [30] when incorporating RR. In the present work, the same RR framework as in [30] was implemented for all HRRT reconstructions, and we investigated quantitatively the additional impact of accurate MC reconstruction on the parameter estimation task. In other words, as depicted in Fig. 2 for a particular PD patient, one commonly observes an increase in BP values when incorporating RR (significance confirmed in [30]) while in this work, we investigate over a range of patients and ROIs, whether additional incorporation of MC further affects the extracted kinetic parameters, as also suggested by Fig. 2.

II. Methods

A. Tomograph

Data were acquired on the second generation Siemens HRRT scanner [5]. The detector heads in the octagonal design consist of a double 10 mm layer of LSO/LYSO for a total of 119,808 detector crystals (crystal size 2.1 x 2.1 x 10 mm^3). The total number of possible LORs is 4.486×10^9.

B. Motion-Tracking

Collection of motion data was carried out using a Polaris motion tracking system (Northern Digital Inc., Waterloo, ON, Canada) [6]. This system uses an infrared signal to track a small tool consisting of four retro-reflective spheres attached to a plastic plate. In subject studies, the Polaris tool was attached to the subjects using a thin neoprene surf cap [12]. These are depicted in Fig. 3.

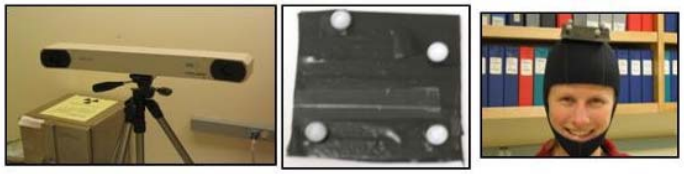

Fig. 3. Depiction of (*left*) the Polaris camera, (*middle*) the tool consisting of four retro-reflective spheres and (*right*) its attachment to the individual via the neoprene cap.

The Polaris camera was mounted approximately 1 m from the rear of the scanner. Calibration of the Polaris frame of reference to that of the tomograph was achieved via a series of simultaneous Polaris and transmission scan measurements of the Polaris tool, as elaborated in [26]. The motion threshold was set to a tenth of the resolution (2.5mm) of the HRRT scanner; having a very high number of motion intervals (Q), does not pose a noticeable increase to the computation task, as explained in [26], due to the image-based nature of performing motion-averages of the sensitivity image (Eq. 4).

C. Clinical FDG imaging

The nearly anatomical nature of FDG images allow for a convenient qualitative inspection of the MC method. To this end, an epileptic 60-year old female subject was scanned for 22min on the HRRT, injected with 10mCi of FDG 90 minutes prior to the scan. In this study (unlike the next), the subject's head was not restrained to the bed (as discussed later). The subject was observed to move considerably in the course of the scan, with standard deviations of 7.3mm, 5.1mm and 0.9mm in the x(horiz.), y(vert.) and z(axial) directions.

D. Dynamic raclopride imaging

Next, we performed a quantitative comparison of reconstructions without and with MC within the context of kinetic parameter estimation in dynamic PET imaging. As described in Sec. I-C, all reconstructions in this study already incorporated RR modeling. Ten subjects with Parkinson's disease (age 59 ± 8) were scanned for 60 minutes on the HRRT scanner, following injection of ^{11}C-raclopride (10.03 ± 0.06 mCi). The data were grouped into 16 time-frames (4x1min, 3x2min, 8x5min, 1x10min) and reconstructed with (i) no MC, (ii) the conventional purely LOR-driven method, and (iii) the investigated MC method (Eq. 4).

1) ROI Placement:: Eight elliptical ROIs were placed on the striatum bilaterally, separating the striatum[1] into caudate (C),

[1]The reason for using multiple ROIs per side is because in PD is that there is a gradient of dopamine loss across the putamen, and an average for the whole structure would not capture that gradient, which is why we use 4 ROIs per side, versus most other groups studying healthy controls who use one or two.

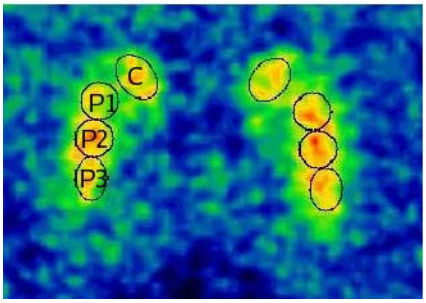

Fig. 4. Depiction of ROIs used in the present analysis.

anterior putamen (P1), intermediate putamen (P2), and posterior putamen (P3), as shown in Fig. 4. The shape and size of each ROI (C = 74.0 mm^2, P1 and P2 = 47.5 mm^2, P3 = 50.5 mm^2) was kept constant throughout image analysis in order to reduce bias and inter-analyst variability. The template shown in Fig. 4 was chosen with reference to the known anatomical shape and size of the striatum, and because it consistently captured the anterior-posterior extent of the striatal signal in the PET images. ROIs were localized on a mean image of the last 1/2 hour of the dynamic PET study in such a way as to maximize the activity contained in each region. These ROIs were then transferred to the dynamic images and TACs were extracted for nine planes averaged into three groups of consecutive planes (10.89 mm). In order to calculate BP values using the Logan method [34], described next, a large elliptical reference ROI was placed on the cerebellum covering an axial extent of 5 planes (6.09 mm).

2) Hypotheses:: Impact of motion-corrected reconstruction on the task of kinetic parameter estimation was investigated via comparisons of:

(i) **BP values:** calculated using a tissue-input Logan [34] analysis with the cerebellum as the reference region (BP = B_{max}/K_d).

(ii) χ^2 **of the time-activity curves:** calculated with respect to a curve fit via the reference tissue model (RTM) [REF]. This model was used, along with the reference cerebellum TAC, to estimate/fit the striatal activity in each ROI across all frames. These estimates were then compared to the measured striatal ROI value to determine the χ^2 value for the entire TAC.

Two hypotheses were tested:

(i) Due to a presumably increased effective resolution for the scanner when performing MC, increased BP values would be obtained[2] (e.g. similar to what one would expect/observe when using higher resolution scanners [29], reconstruction methods with resolution recovery [30] and/or partial volume correction methods [1], [28]).

(ii) Due to a presumably greater accuracy in the quantitative measurement process, decreased χ^2 values would be obtained when performing MC; in other words, the biological model would be able to better fit the MC data. This is also related to the fact that when performing MC, the TACs become more continuous (i.e. with less abrupt changes) as the ROIs capture the same anatomic regions across all frames, unlike the case without MC in which the ROIs can be misplaced in motion impacted frames.

[2]The reduction in motion-induced blurring when performing MC is also accompanied by an implicit frame-to-frame realignment. The former is certainly expected to increase the BP values, while the effect of the latter, and its importance, will depend on how the TACs are modified and where the data are most over/under-estimated prior to MC.

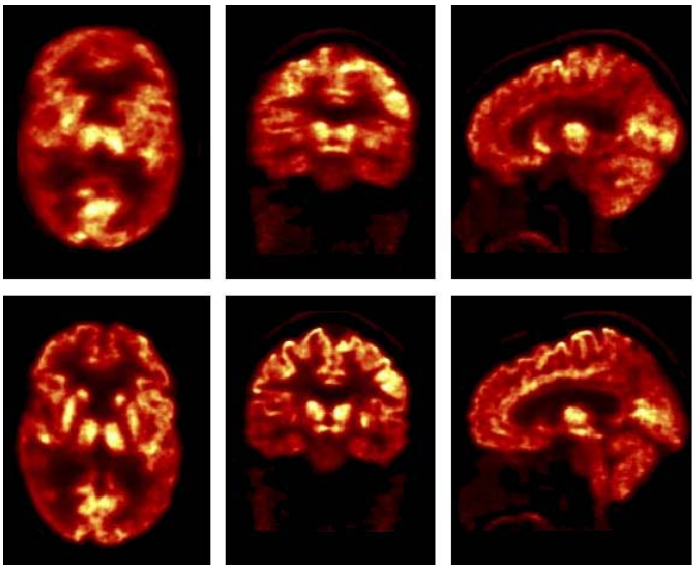

Fig. 5. Transaxial (first column), coronal (second column) and sagittal (third column) slices across the striatum reconstructed without (top row) and with (bottom row) motion correction scheme investigated in this work.

3) Statistical Analysis: The above hypotheses were tested by comparing BP and χ^2 values calculated without and with MC, via the directional Wilcoxon non-parametric matched-pair signed-rank test using exact critical values as tabulated by McCornack [3] [32]. This comparison was done for the overall striatal region as well as individuals striatal ROIs. Similar to [30], the Wilcoxon measure was selected since the distributions are not known to be Gaussian in nature. For comparison purposes however, we have also performed the analysis using the standard paired t-test, which does assume a Gaussian distribution.

III. Results and Discussion

A. FDG Imaging

FDG images of the epileptic subject, reconstructed without and with MC are shown in Fig. 5. Very clear improvements in effective image resolution can be inferred from the superior quality obtained with the MC reconstruction. The tracer uptake is reconstructed such that the cortex, striatum and thalamus are clearly delineated in the MC image. This agrees with our previous validation studies that simulated motion impacted

[3]The author has shown that the normal approximation to the Wilcoxon distribution, proposed in [33], result in errors less than 10% for $35<N<100$ at the 0.5, 0.25, 0.025 and 0.005 one-tail probability levels (though not at the 0.0005 level). For all N values in this work (6, 10, 80), we have used the exact values for best accuracy, and performed linear interpolation for probability levels α not in the table.

human brain data [26], where clear improvements in contrast (a measure of effective resolution) versus noise were obtained. Our ability to accurately compensate for motion occurring during PET scanning, as in the case of the epileptic subject studies here, indicates that there is a strong possibility of performing clinical scans with minimal to no head restraint. This would contribute greatly to the comfort of study subject during scanning. In the next part, we look more closely at quantitative results from dynamic studies of longer duration.

B. Dynamic Raclopride Imaging

Motion data were recorded for a group of ten subjects (see Sec. II-D) in order to incorporate this information into the reconstruction process. The measured motion coordinates for a particular PD subject, over the course of an hour long scan, are shown in Fig. 6. Figs. 6A, 6B and 6C show the subject's displacement along the x (horizontal), y (vertical) and z (axial) directions, respectively, in the center of the cerebellum, occipital cortex and striatum. Fig. 6D plots the rotations measured in reference to the position of the tool at the start of the scan.

Various states of the subject are labeled in Fig. 6, allowing correlation of motion magnitudes with visually observed subject activities. In particular, as part of the investigation protocol, 40 minutes into the emission scan a physician evaluated the subject's symptoms using a modified version (no head or neck observations) of the Unified Parkinson's Disease Rating Scale (UPDRS) requiring the subject to speak and move both their arms and legs [31], labeled as 'evaluation' in the figures.

Fig. 7 depicts a typical set of images for a subject reconstructed using (i) no MC, (ii) the purely LOR-driven method, and (iii) the investigated MC method. Artifacts are visible for the second scenario (middle row) as previously predicted and observed in phantom and simulation studies [26], and can be attributed to a lack of appropriate modeling (see Sec. I). Due to its inferior performance, this method will not be considered further.

1) BP analysis:: BP values obtained without and with MC were compared for all the 10 subjects as well as a subset of subjects (6 of 10) that exhibited "High Motion" (HM): defined as those studies in which the striatum underwent a maximum absolute displacement larger than the resolution of the scanner (2.5mm). This subset of the data, unlike the rest, exhibited motion with an overall standard deviation σ of greater than 0.6mm, obtained by averaging the three standard deviation values $\sigma_{x/y/z}$ of displacement coordinates in all the 3 directions at the center of the cerebellum). The resulting BP values are depicted in Fig. 8. The relatively increased values, more apparently the case for the HM studies, were predicted and can be explained by a higher effective resolution when performing MC (see Sec. II-D.2), which we quantify next.

Probability levels α for the null hypothesis, as obtained by the Wilcoxon measure (see Sec. II-D.2), are summarized in Table I, with * indicating $p<0.05$. For the overall ten-subjects study, a consistent and noticeable pattern of increase in the

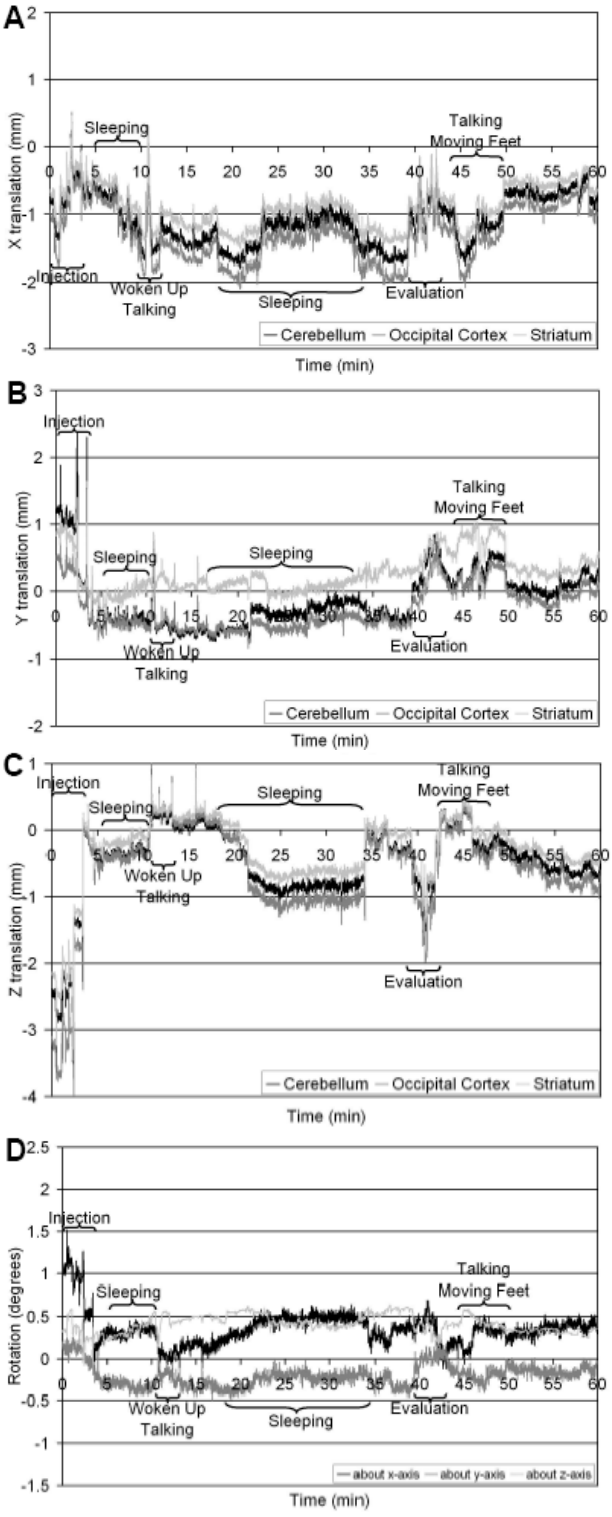

Fig. 6. Displacements made by a PD subject wearing a thermoplastic mask restraint, along the x/horizontal (A), y/vertical (B) and z/axial (C) axes. Corresponding rotations about all three axes are also shown (D).

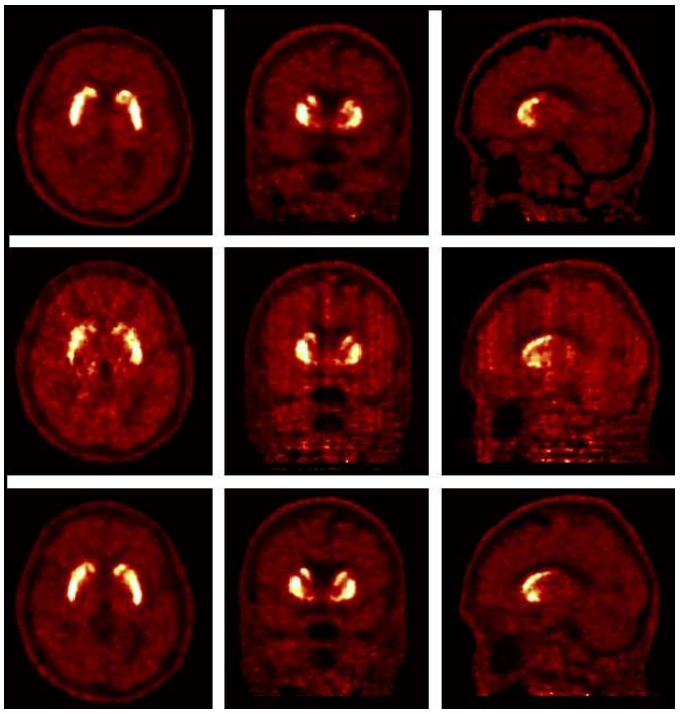

Fig. 7. Slices across the striatum for reconstructions (frames 7-13: 10-45min) without MC (*first row*), with purely event-driven MC (*second row*) and with the investigated MC (*third row*) methods. Clear artifacts can be seen with the purely event-driven approach. The investigated MC method results in better visual separation of caudate and putamen.

TABLE I

TABLE OF PROBABILITY LEVELS α FOR WHICH P$<\alpha$ (* INDICATES P$<$0.05).

ROI	Wilcoxon All (N=10)	Wilcoxon HM (N=6)	t-test All (N=10)	t-test HM (N=6)
Left C	*0.025	*0.038	*0.031	*0.036
Right C	*0.015	*0.050	*0.017	*0.049
Left P1	*0.020	*0.038	*0.017	*0.016
Right P1	*0.015	*0.038	*0.012	*0.008
Left P2	0.063	*0.038	0.059	*0.020
Right P2	*0.015	*0.038	*0.014	*0.017
Left P3	0.075	*0.038	*0.039	*0.032
Right P3	0.063	*0.038	0.059	*0.048
ROIs Combined	*0.0001	*0.0001	*0.0001	*0.0001

BP values was noted for all 8 ROIs, five of which showed a significant increase in BP (p$<$0.05). For the "High Motion" studies, the increases became significant (p$<$0.05) for *all* the ROIs, as expected since MC is more important when motion is larger. Comparison of BP values obtained from images without and with MC across all subjects and all ROIs (i.e. N=80) showed a very high level of significance (p$<$0.0001). For comparison purposes (see discussion in Sec. II-D.2), α values obtained using the standard t-test are also shown, and in most cases indicate a slightly higher level of significance.

2) χ^2 analysis:: Some typical TACs are shown in Fig. 9 without and with application of MC. For the TACs shown, one

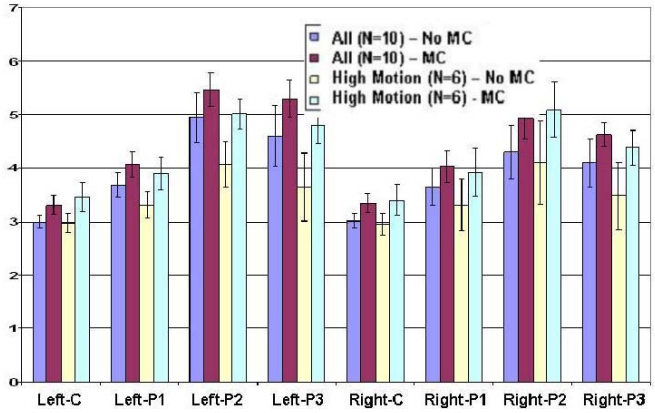

Fig. 8. BP values without and with MC for the entire dataset (10 subjects) as well as subjects exhibiting "high motion" (see text).

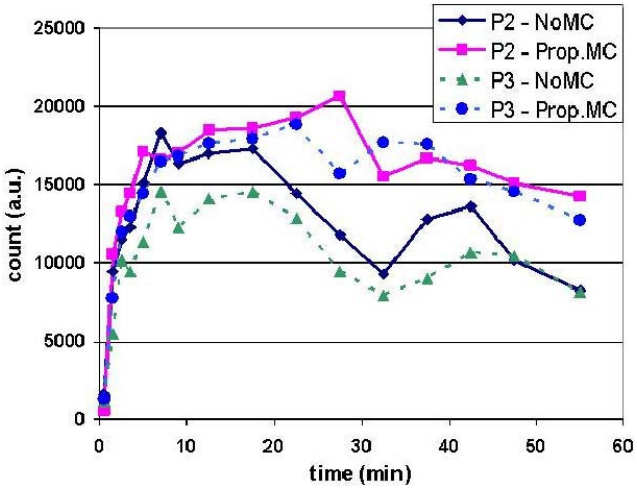

Fig. 9. Right/left-averaged P2 and P3 TACs for a particular subject.

observes increases in the values (similar to what is typically observed in partial-volume correction [2]) with MC. Additionally, less variability can be detected in the TACs, as predicted in Sec. II-D, which we quantify next.

A significant (p$<$0.05 Wilxocon, p$<$0.013 t-test) decrease was observed when comparing the variability of the TACs without and with motion correction over all (N=80) subjects and ROIs (not shown). Investigating these changes on an ROI level, the impact on striatal variability was attributed to the right and left P3 TACs (shown in Fig. 10), exhibiting significant reductions (p$<$0.025 Wilxocon, p$<$0.019 t-test for right P3 and p$<$0.01 Wilxocon, p$<$0.013 t-test for left P3). For the HM studies, the levels of significance did not improve additionally.

The significant effect of increased accuracy for the P3 region when performing MC can be attributed to the TACs obtained for this region being especially prone to non-continuities caused by movements along the subject axis, since the P3 ROIs can easily start to incorporate surrounding tissue as they move off the bottom of the structure in some frames. Additionally, this region is narrower than the rest of the striatum such that right/left

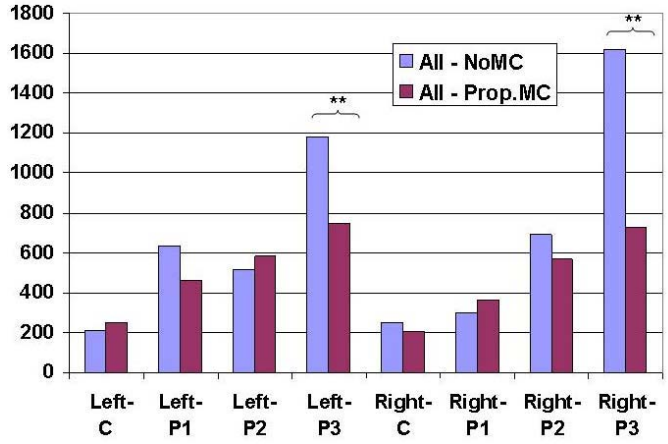

Fig. 10. Plots of TAC χ^2 for RTM model fitting: significant decreases (** indicates p<0.025) are observed for the right and left posterior putamen (P3) ROIs, as summarized in the text.

movements will have more noticeable effects.

It must be noted that validation of this hypothesis is consistent with observations made in [4], when examining other MC methods[4], that demonstrated improved test-retest reliability (i.e. reduced variability). This is because, a significant decrease in fitting errors (as investigated in this work using the χ^2 measure) when using appropriate biological models to extract dynamic variables such as the BP, would predict decreased variability in those variables.

Future studies will investigate cases where a biological change is expected, for example before and after administration of a drug promoting dopamine release, across a large group of subjects. It is expected that motion corrected images will yield results that will better reflect this known biological change.

IV. Conclusion

In this work, the qualitative and quantitative impact of an accurate event-driven MC statistical reconstruction on imaging of PET subjects was investigated. In the context of clinical imaging, the possibility of performing scans with minimal to no head restraint was indicated, wherein the data from an epileptic subject, with no head constraint at all, were reconstructed incorporating MC to produce images of superior quality and clear anatomical delineation.

In the context of dynamic PET kinetic parameter estimation, BP values were seen to increase consistently and noticeably across all eight striatal regions from which they were extracted (all with p<0.075, five of which were with p<0.05), being attributed to the increased effective resolution of the scanner due to MC. A higher level of significance was observed for BP values derived from the subset of subjects exhibiting maximum absolute displacement above the resolution (2.5mm) of the HRRT scanner; i.e. as expected we observed more significant BP increases with higher degrees of movements. Additionally, comparing changes in BP with and without MC across all subjects and ROIs, a highly significant increase was observed (p<0.0001).

Furthermore, the variability in the TACs, measured using the χ^2 measure and extracted across all subjects and ROIs, decreased significantly (p<0.05) with the use of the MC technique. This reduction was primarily attributed to significant decreases in variability of TACs generated in each of the right and left posterior putamen (p<0.025). We thus conclude that our implementation of accurate event-driven MC within the context of statistical reconstruction significantly impacts the estimated dynamic PET kinetic parameters.

[4]In [4], method(s) that fully address issues raised in Sec. I are not utilized; rather the purely event-driven approach is used, as well as a particular frame-by-frame variation of it that is intended to minimize potentially adverse effects of those issues.

Acknowledgments

This work was supported by the National Institute of Health (grant #'s: DA00412 and S10RR017219), the TRIUMF Life Science Grant, the Natural Sciences and Engineering Research Council of Canada, and the Michael Smith Foundation for Health Research. The authors wish to thank Andrew Crabb, Kelvin Raywood and Ken Buckley for considerable computational and technical support in the course of this work.

References

[1] O. Mawlawi, D. Martinez, M. Slifstein, A. Broft, R. Chatterjee, D. Hwang, Y. Huang, N. Simpson, K. Ngo, R. Van Heertum, and M. Laruelle, "Imaging Human Mesolimbic Dopamine Transmission With Positron Emission Tomography: I. Accuracy and Precision of D2 Receptor Parameter Measurements in Ventral Striatum", *Cereb. Blood Flow Metab.*, vol. 21, pp. 1034-1057, 2001.

[2] O. G. Rousset, P. Deep, H. Kuwabara, A. C. Evans, A. H. Gjedde, P. Cumming P, "Effect of partial volume correction on estimates of the influx and cerebral metabolism of 6-[F-18]fluoro-L-dopa studied with PET in normal control and Parkinson's disease subjects" , *Synapse*, vol. 37, pp. 81-89, 2000.

[3] K. Thielemans, S. Mustafovic, and L. Schnorr, "Image Reconstruction of Motion Corrected Sinograms", *IEEE NSS/MIC Conf. Record*, vol. 4, pp. 2401-2406, 2003.

[4] A. J. Montgomery, K. Thielemans, M. A. Mehta, F. Turkheimer, S. Mustafovic, and P. M. Grasby, "Correction of Head Movement on PET Studies: Comparison of Methods", *J. Nucl. Med.*, vol. 47, pp. 1936-1944, 2006.

[5] V. Sossi, H.W.A.M. de Jong, W. C. Barker, P. Bloomfield, Z. Burbar, M-L. Camborde, C. Comtat, L. A. Eriksson, S. Houle, D. Keator, C. Knob, R. Krais, A. A. Lammertsma, A. Rahmim, M. Sibomana, M. Teras, C. J. Thompson, R. Trebossen, J. Votaw, M. Walker, K. Wienhard, D. F. Wong,, "The second generation HRRT - a multi-centre scanner performance investigation", *IEEE NSS/MIC Conf. Record*, vol. 4, pp. 23-29, 2005.

[6] B. J. Lopresti, A. Russo, W. F. Jones, T. Fisher, D. G. Crouch, D. E. Altenburger, D. W. Townsend, "Implementation and Performance of an Optical Motion Tracking System for High Resolution Brain PET Imaging", *IEEE Trans. Nucl. Sci.*, vol. 46, pp. 2059-2067, 1999.

[7] Y. Picard, and C. J. Thompson, "Motion correction of PET images using multiple acquisition frames", *IEEE Trans. Med. Imag.*, vol. 16, pp. 137-144, 1997.

[8] J. Qi and R. M. Leahy, "Resolution and noise properties of MAP reconstruction for fully 3-D PET", *IEEE Trans. Med. Imag.*, vol. 19, pp. 493-506, 2000.

[9] M. Reyes, G. Malandain, P. M. Koulibaly, M. A. Gonzalez-Ballester, and J. Darcourt, "Model-based respiratory motion compensation for emission tomography image reconstruction", *Phys. Med. Biol.*, vol. 52, pp. 3579-3600, 2007.

[10] E. Ü. Mumcuoğlu, R. M. Leahy, S. R. Cherry, and Z. Zhou, "Fast Gradient-Based Methods for Baysian Reconstruction of Transmission and Emission PET Images", *IEEE Trans. Med. Imag.*, vol. 13, pp. 687-701, 1994.

[11] A. J. Reader, S. Ally, F. Bakatselos, R. Manavaki, R. Walledge, A. P. Jeavons, P.J.Julyan, S. Zhao, D. L. Hastings and J. Zweit, "One-Pass List-Mode EM Algorithm for High-Resolution 3-D PET Image Reconstruction Into Large Arrays", *IEEE Trans. Nucl. Sci.* vol. 49, pp. 693-699, 2002.

[12] P. M. Bloomfield, T. J. Spinks, J. Reed, L. Schnorr, A. M. Westrip, L. Livieratos, R. Fulton, and T. Jones, "The design and implementation of a motion correction scheme for neurological PET", *Phys. Med. Biol.*, vol. 48, pp. 959-978, 2003.

[13] F. Qiao, T. Pan, J. W. Clark, and O. R. Mawlawi, "A motion-incorporated reconstruction method for gated PET studies", *Phys. Med. Biol.*, vol. 51, pp. 3769-3783, 2006.

[14] T. Li, B. Thorndyke, E. Schreibmann, Y. Yang, and L. Xing, "Model-based image reconstruction for four-dimensional PET", Med. Phys., vol. 33, pp. 1288-1298, 2006.

[15] F. Lamare, M. J. Ledesma Carbayo, T. Cresson, G. Kontaxakis, A. Santos, C. Cheze Le Rest, A. J. Reader and D. Visvikis, "List-mode-based reconstruction for respiratory motion correction in PET using non-rigid body transformations", *Phys. Med. Biol.*, vol. 52, pp. 5187-5204, 2007.

[16] T. Beyer, L. Tellmann, I. Nickel, U. Pietrzyk, "On the use of positioning aids to reduce misregistration in the head and neck in whole-body PET/CT studies", J. Nucl. Med. vol. 46, pp. 596-602, 2005.

[17] R. R. Fulton, S. R. Meikle, S. Eberl, J. Pfeiffer, and C. J. Constable, "Correction for head movement in positron emission tomography using an optical motion tracking system", *IEEE Trans. Nucl. Sci.*, vol. 49, pp. 116-123, 2002.

[18] A. Rahmim, M. Lenox, A. J. Reader, C. Michel. Z. Burbar, T. J. Ruth, and V. Sossi, "Statistical list-mode image reconstruction for the high resolution research tomograph", Phys. Med. Biol., vol. 49, pp. 4239-4258, 2004.

[19] A. Rahmim, J. C. Cheng, S. Blinder, M-L. Camborde, and V. Sossi, "Statistical dynamic image reconstruction in state-of-the-art high resolution PET", *Phys. Med. Biol.*, vol. 50, pp. 4887-4912, 2005.

[20] M. Menke, M. S. Atkins, and K. R. Buckley, "Compensation Methods for Head Motion Detected During PET Imaging", *IEEE Trans. Nucl. Sci.*, vol. 43(1), pp. 310-317, 1996.

[21] M. E. Daube-Witherspoon, Y. C. Yan, M. V. Green, R. E. Carson, K. M. Kempner, and P. Herscovitch, "Correction for motion distortion in PET by dynamic monitoring of patient position (Abstract)", *J. Nucl. Med.*, vol. 31, pp. 816, 1990.

[22] J. Qi and R. H. Huesman, "List mode reconstruction for PET with motion compensation: a simulation study", *Proc. IEEE Inter. Symp. Bio. Imag.*, pp. 413-416, 2002.

[23] P. Buehler, U. Just, E. Will, J. Kotzerke, and J. van den Hoff, "An Accurate Method for Correction of Head Movement in PET.", *IEEE Trans. Med. Imag.*, vol. 23(8), pp. 1176-1185, 2004.

[24] A. Rahmim, P. Bloomfield, S. Houle, M. Lenox, C. Michel, K. R. Buckley, T. J. Ruth, and V. Sossi, "Motion compensation in histogram-mode and list-mode EM reconstructions: beyond the event-driven approach", *IEEE Trans. Nucl. Sci.*, vol. 51, pp. pp. 2588-2596 (2004).

[25] A. Rahmim, J. C. Cheng, K. Dinelle, M. A. Shilov, W. P. Segars, O. G. Rousset, B. M. W. Tsui, D. F. Wong, and V. Sossi, "System Matrix Modeling of Externally Tracked Motion", *IEEE Med. Imag. Conf. Records*, vol. 4, pp. 2137-2141, 2006.

[26] A. Rahmim, K. Dinelle, J. C. Cheng, M. A. Shilov, W. P. Segars, S. C. Lidstone, S. Blinder, O. G. Rousset, H. Vajihollahi, B. M. W. Tsui, D. F. Wong, V. Sossi, "Accurate Event-Driven Motion Compensation in High-Resolution PET Incorporating Scattered and Random Events", submitted to *IEEE Trans. Med. Imag.*, 2007.

[27] A. Rahmim, O. G. Rousset, H. Zaidi, "Strategies for motion tracking and correction in PET", *Pet Clinic*, 2007 (exact reference to be added)

[28] H. Kuwabara, O. Rousset, A. Kumar, W. Ye, J. R. Brasic, D. F. Wong, "Evaluation of tissue homogeneity assumptions of partial volume correction for [11C]raclopride binding potential volumes", *J. Nucl. Med.*, vol. 47, pp. 192P, 2006.

[29] Y. Zhou, M. Weed, M-K. Chen, A. Rahmim, W. Ye, J. Brasic, M. Alexander, A. Crabb, J. McGlothan, F. Ali, T. Guilarte, and D. Wong, "Quantitative dopamine transporter imaging studies in nonhuman primates with a GE Advance and high resolution research tomography (HRRT) PET scanners", J. Nucl. Med., vol. 48, pp. 158P, 2007.

[30] F. C. Sureau, C. Comtat, A. J. Reader, C. Leroy, M. J. Santiago-Ribeiro, I. Buvat, and R. Trebossen, "Improved Clinical Parametric Imaging Using List-Mode Reconstruction via Resolution Modeling", *IEEE NSS/MIC Conf. Record*, vol. 6, pp. 3507-3510, 2006.

[31] S. Fahn, and R. L. Elton, "Unified Parkinsons's Disease Rating Scale", in: S. Fahn, C. D. Mardsen, D. Calne, M. Goldstein, eds. Recent Developments in Parkinson's Disease, Volume 2. New Jersey: MacMillan Health Care Information; 1987:153-163.

[32] R. L. McCornack, "Extended Tables of the Wilcoxon Matched Pair Signed Rank Statistic", *J. Amer. Stat. Assoc.*, vol. 60, pp. 864-871, 1965.

[33] F. Wilcoxon, "Individual comparisons by ranking methods",*Biometrics Bulletin*, vol. 1, pp. 119-122, 1947.

[34] J. Logan, J. S. Fowler, N. D. Volkow, G-J. Wang, Y-S Ding, and D. L. Alexoff, "Distribution Volume Ratios Without Blood Sampling from Graphical Analysis of PET Data", *J. Cereb. Blood Flow Metab.*, vol. 16, pp. 834, 1996.

[35] H. Herzog, L. Tellmann, R. Fulton, I. Stangier, E. Rota Kops, K. Bente, C. Boy, R. Hurlemann, and U. Pietrzyk, "Motion Artifact Reduction on Parametric PET Images of Neuroreceptor Binding", *Journ. Nucl. Med.*, Vol. 46, pp. 1059-1065, 2005.